SCIENTIFIC REP🞖RTS

Efficient Photocatalytic Activities of TiO₂ Hollow Fibers with Mixed Phases and Mesoporous Walls

Huilin Hou[1,2], Minghui Shang[2], Lin Wang[2], Wenge Li[3], Bin Tang[1] & Weiyou Yang[2]

Currently, Degussa P25, with the typical mixed phases of anatase and rutile TiO₂, is widely applied as the commercial photocatalysts. However, there are still some of obstacles for the P25 nanoparticles with totally high photocatalytic activities, especially for the catalytic stability due to their inevitable aggregation of the nanoparticles when used as the photocatalysts. In the present work, we reported the exploration of a novel TiO₂ photocatalyst, which could offer an ideal platform for synergetic combination of the mixed-phase composition, hollow architecture and mesoporous walls for the desired excellent photocatalytic efficiency and robust stability. The mesoporous TiO₂ hollow nanofibers were fabricated via a facile single capillary electrospinning technique, in which the foaming agents were used for creating mesopores throughout the walls of the hollow fibers. The obtained hollow fibers exhibit a high purity and possess the mixed phases of 94.6% anatase and 5.4% rutile TiO2. As compared to P25, the as-fabricated mesoporous TiO2 hollow fibers exhibited much higher efficient photocatalytic activities and stabilities toward the hydrogen evolution with a rate of ~499.1 μmol g^{-1}·h^{-1} and ~99.5% degradation Rhodamine B (RhB) in 60 min, suggesting their promising application in efficient photocatalysts.

Semiconductor photocatalyst materials are extensively explored for the solar energy utilization, which offer a possible strategy to address the environmental problem and energy crisis[1,2]. Up to date, numerous interests have been focused on the titanium dioxide (TiO₂) material, due to its low cost, ready commercial availability, and long-term stability against the photochemical corrosion in aggressive aqueous environments[3,4].

Generally, TiO₂ has four typical allotropic forms including anatase, brookite, rutile, and TiO₂(B), among which the anatase has been considered as the one with the best photoactivity[5]. Compared with the pure TiO₂ material, the mixed-phase TiO₂ photocatalysts such as commercial Degussa P25 (composed by ~80% anatase and ~20% rutile) and anatase/TiO₂(B) fibers, can exhibit much higher photocatalytic activity[6–11], which could be mainly attributed to the enhanced charge transfer caused by the energy difference between the conduction band (CB) edges of two phases. In addition to the TiO₂ crystallinity, porous structure of the photocatalyst is beneficial for the adsorption of the reactants, and thus can significantly improve the photocatalytic efficiencies. For example, one-dimensional (1D) TiO₂ hollow structures are of great interest in the viewpoint of their potential various applications and fundamental phenomena specific to a confined nanostructure[12–17]. Particularly, the hollow TiO₂ fibers with designed mesoporous walls have received remarkable attention owing to their unique hierarchical pore structure, which is helpful for improved capabilities of mass transport through the material body and maintenance of a specific surface area on the level of a satisfactory porosity[18–22]. That is to say, the efficient photocatalytic activities of the TiO₂ semiconductors could be expected, once they are grown into the fiber structures together with hollow bodies, mixed phases and mesoporous walls. However, the reported works often suffered

[1]Research Institute of Surface Engineering, Taiyuan University of Technology, Taiyuan City, 030024, P.R. China. [2]Institute of Materials, Ningbo University of Technology, Ningbo City, 315016, P.R. China. [3]Merchant Marine College, Shanghai Maritime University, Shanghai City, 201306, P.R. China. Correspondence and requests for materials should be addressed to B.T. (Email: tangbin@tyut.edu.cn) or W.Y. (Email: weiyouyang@tsinghua.org.cn)
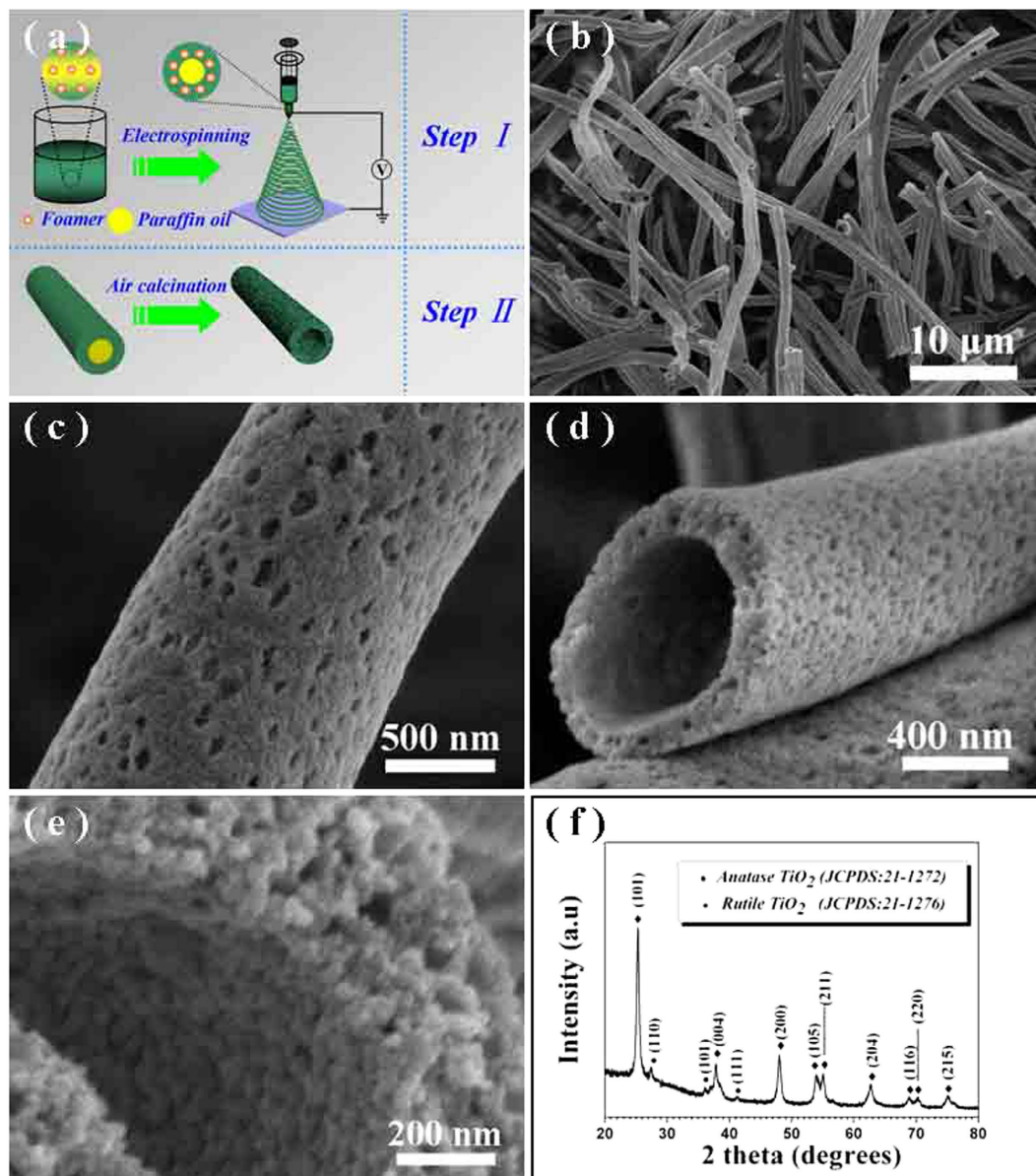
Figure 1. (**a**) Schematic illustration for the formation of mesoporous TiO$_2$ hollow fibers via the foaming assisted electrospinning. (**b**) A typical SEM image of the calcined products under a low magnification. (**c–e**) Typical SEM images of the calcined products under higher magnifications and different views. (**f**) A representative XRD pattern of the calcined products.

from tedious procedures or special conditions. Thereby, it is still a challenge for developing a simple and facile route to generate mesoporous TiO$_2$ hollow nanofibers.

In the present work, we report the exploration of a novel TiO$_2$ photocatalyst, which could offer an ideal platform for synergetic combination of the mixed-phase composition, hollow architecture and mesoporous walls for the desired excellent photocatalytic efficiency and long-term stability. The mixed-phase anatase/rutile TiO$_2$ hollow fibers are fabricated via a simple electronspinning method. As illustrated in Fig. 1(a), the hollow structures are obtained by removing the inside paraffin oil during the air calcination, and the foaming agents (DIPA) are concomitantly decomposed into abundant vapor phases to create the thoroughly mesoporous walls. As expected, the obtained hollow fibers, with the mixed phases of anatase and rutile TiO$_2$ as well as mesoporous walls exhibit excellent photocatalytic performances in hydrogen production and dye degradation under UV light irradiation.

Methods

Raw materials. Polyvinylpyrrolidone (PVP, $M_W \approx 1300000$), butyl titanate (TBOT), diisopropyl azodiformate (DIPA), paraffin oil, absolute ethyl alcohol, acetic acid, deionized water and rhodamine B (RhB)

were purchased from Aladdin (Shanghai, China). All materials were directly used as received without further treatment.
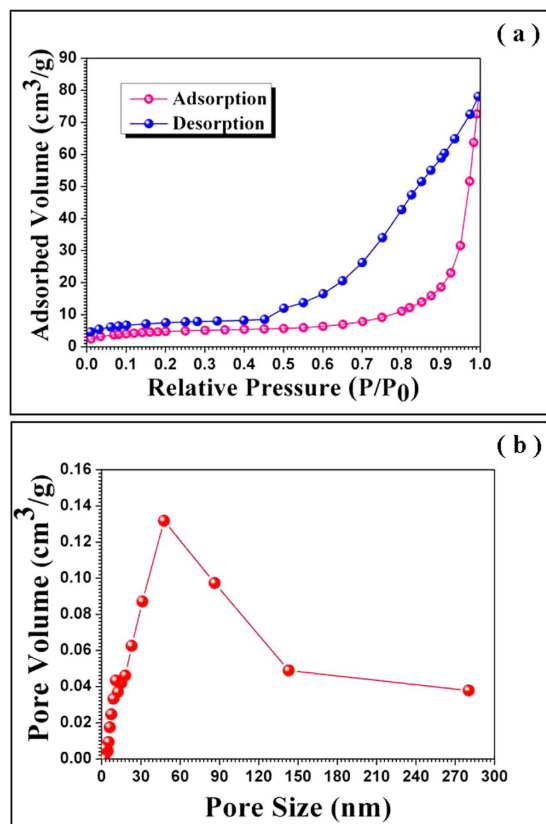
Preparation of msoporous TiO$_2$ hollow fibers.   In a typical experimental procedure, 0.6 g of PVP, 3.0 g of TBOT and 0.5g of DIPA were firstly dissolved in 7 mL absolute ethyl alcohol with stirring vigorously for 2 h. Then, 0.5 g of CTAB and 2 ml paraffin oil were added into the above solution followed by being subjected to the magnetic stirring further for 5 h. Subsequently, the above precursor microemulsions were transformed into a plastic syringe with a stainless steel nozzle (anode, diameter: 0.2 mm). The tip of the stainless steel nozzle was placed in the front of a metal cathode (collector) with a fixed distance of 20 cm between the nozzle and the collector. An electrical potential of 18 kV and a flow rate of 1 mL h^{-1} were applied for electrospinning precursor fibers. The as-spun polymer fibers were dried in an oven at 60 °C, followed by being located in a quartz crucible and placed at the center of a conventional tube furnace. Finally, the precursor fibers were heated up to the desired temperature of 500 °C with a heating rate of 1 °C min^{-1}, and maintained there for 3 h in air, followed by furnace-cool to ambient temperature.

Structure characterization.   The obtained products were characterized with X-ray powder diffraction (XRD, D8 Advance, Bruker, Germany) with Cu Kα radiation ($\lambda = 1.5406$ Å), field emission scanning electron microscopy (FESEM, S-4800, Hitachi, Japan), and high-resolution transmission electron microscopy (HRTEM, JEM-2010F, JEOL, Japan) equipped with energy dispersive X-ray spectroscopy (EDX, Quantax-STEM, Bruker, Germany). The porous properties of the as-prepared mesoporous fibers were characterized using N$_2$ adsorption at -195.8 °C on a specific surface area and porosity analyzer (ASAP 2020HD88, Micromeritics, USA).

Photocatalytic activity measurements.   The photocatalytic activities of the resultant products were firstly evaluated for hydrogen evolution. The photocatalytic reaction is performed in an inner-irradiation quartz annular reactor with a 300 W Xenon lamp (CEL, HUL300), a vacuum pump, a gas collection, a recirculation pump and a water-cooled condenser. The as-synthesized samples (0.1 g) were suspended in deionized water and methanol mixed solutions (40 mL, 3:1) by an ultrasonic oscillator, respectively. Then the mixture was transferred into the reactor and deaerated by the vacuum pump. The Xenon lamp was utilized as a light source, and the cooling water was circulated through a cylindrical Pyrex jacket located around the light source to maintain the reaction temperature. The reactor was sealed with ambient air during irradiation, and the hydrogen evolution were monitored by an online gas chromatography (GC, 7900) equipped with a Porapak-Q column, high-purity nitrogen carrier and a thermal conductivity detector (TCD). In order to investigate the stability and recyclability, the products were re-used in the same reaction for 3 cycles. Furthermore, degradation of rhodamine B (RhB, Aladdin, Shanghai, China) was studied to evaluate its photocatalytic ability. The photocatalytic reaction is performed at an inner-irradiation quartz annular reactor, which has a Xenon lamp ($\lambda > 320$ nm, CEL-Hx F300, Beijing, China) and a water-cooled condenser. Typically, 1.2 mg of RhB and 40 mg of the as-prepared catalysts were dispersed in 120 ml deionized water. Prior to irradiation, the suspensions were magnetically stirred in the dark for 60 min to ensure the establishment of an adsorption-desorption equilibrium between the photocatalyst and the RhB dye. An aliquot (3 mL) of the solution was taken at a certain time interval (10 min) during the reaction and analyzed on the UV-visible spectrophotometer as mentioned above. The change in RhB absorbance in the solution was used to monitor the extent of reaction at the given irradiation time intervals. For comparison, Degussa P25 was commercially available, and used directly for the photocatalytic activity for H$_2$ generation and degradation of RhB.

Results

SEM was firstly employed to meticulously study the morphology and microstructure of the precursor fibers and their corresponding calcined products. The resultant precursor fibers (Figure S1 (a), Supplementary Information) are continuous with the diameters in the range of $1 \sim 1.5 \mu m$ and up to several hundred of millimeters in length. Figure 1(b–e) are the typical SEM images under different magnifications and views of the corresponding calcined products. It seems that the long continuous precursor fibers have been converted into hollow structures with the diameters reduced to ~900 nm, which could be mainly ascribed to the elimination of the organisms during the air calcination process (see Fig. 1(b)). Figure 1(c–e) show the interior and external surface view under different magnifications of the TiO$_2$ hollow fibers, respectively, disclosing that numerous pores exist on the fiber surface and the hollow fiber walls are thoroughly mesoporous. The formation of the hollow and mesoporous structures could be mainly attributed to the decomposition and removing of organics existed within the as-spun polymeric fibers. The powder X-ray diffractograms (XRD) in wide angles are used to characterize the phase compositions of the calcined products. As shown in Fig. 1(f), besides the dominant diffraction peaks of anatase TiO$_2$ (JCPDS, No. 21-1272), some weak diffraction peaks of rutile phase (JCPDS, No. 21-1276) can be also clearly detected, suggesting that the obtained products possess the mixed phases of anatase and rutile TiO$_2$. According to the XRD data, these two phases existed in the fibers can be calculated by using semi-quantitative calculation method, disclosing that the as-synthesized hollow TiO$_2$ fibers are composed of 94.6% anatase and 5.4% rutile. As mentioned above, the mixed-phase structure favors the exploration of efficient photocatalysts, since the photogenerated charge transfer between the

Figure 2. (**a**) Nitrogen adsorption-desorption isotherm curve of mesoporous TiO_2 hollow nanofibers. (**b**) Pore size distribution curve of the mesoporous TiO_2 hollow nanofibers.

involved two phases can greatly inhibit the charge recombination of the holes/electrons, thus leading to the enhancement of the photocatalytic activities[23–25].

The nitrogen adsorption measurements (Fig. 2(a) reveal that the as-fabricated products exhibit the type IV isotherm behavior with H3 hysteresis, implying that the obtained hollow fibers are mesoporous with a BET surface area of ~27.2 m^2/g. According to the Barrett–Joyner–Halenda (BJH) pore size distribution analysis determined from the adsorption branches (Fig. 2(b)), the average BJH pore diameter is centered at ~38 nm.

TEM was further used to investigate the structural details of the mixed-phase hollow fiber, as shown in Fig. 3(a). In agreement with the SEM observations, the inner tunnel is clearly observed by the sharp contrast between TiO_2 mesoporous wall and the hollow interior. The wall thickness and inner diameter are ~100 nm and ~215 nm, respectively, suggesting the large exposed surface of the products. Figure 3(b) presents the corresponding selected area electron diffraction (SAED) pattern recorded from the single fiber in Fig. 3(a), suggesting its polycrystalline nature. The dominant diffraction spot rings could be sequentially indexed to the crystal planes of (101), (004), (105), (200) and (204) of anatase TiO_2 (JCPDS, No. 21-1272), and the low-intensity diffraction spot ring matches to the (110) plane of rutile TiO_2 (JCPDS, No. 21-1276). Furthermore, a representative high-resolution TEM (HRTEM) image (Fig. 2(c)) recorded from the marked area in Fig. 3(a) discloses the mixed-phase structures existed within the hollow fiber bodies. Accordingly, the two fast fourier transformation (FFT) images (Fig. 3(d,e)) provide the electron diffraction signals corresponding to the local lattice patterns recorded from the marked areas of A and B in Fig. 3(c), respectively. Their crystalline structure and crystalline face are determined from the distances between the reciprocal lattice points and center point in the FFT images[23], implying that both squared regions possess the tetragonal characteristic. Hoverer, the measured distance between the highest intensity point and center one is unequal, suggesting the different phases of these two given selected areas, where the marked areas of A and B belong to anatase (the inset of Fig. 3(d)) and rutile (the inset of Fig. 3(e)), respectively. Figure 3(f,g) are the corresponding fast flourier transformation images (IFFT), further confirmed that d-spacing of 0.35 nm matches to the (101) plane of anatase (Fig. 3(f)) and that of 0.32 nm corresponds to the (110) plane of rutile (Fig. 3(g)), respectively. This is in good agreement with the XRD diffraction results, confirming that the obtained products should be composed by the mixed-phase of anatase and rutile TiO_2. The energy-dispersive X-ray (EDX) spectroscopy analyses (typically shown in Figure S2, Supplementary Information), recorded from a number of fibers and different positions along a single one, suggest that the chemical compositions are identical and mainly
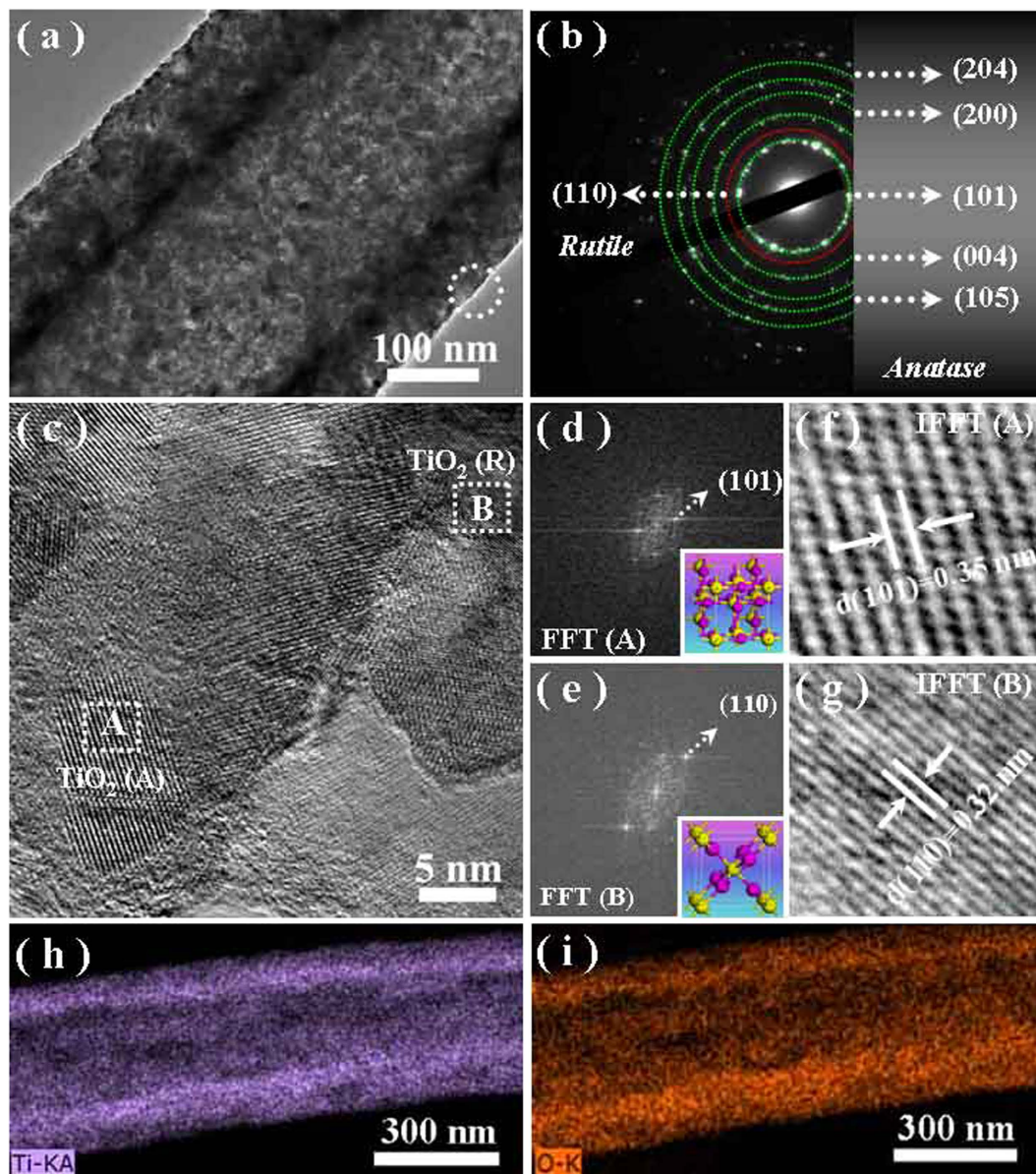
Figure 3. (**a**) A representative TEM image of the mesoporous TiO_2 hollow fibers. (**b**) The corresponding SAED pattern. (**c**) A representative HRTEM image of the mesoporous hollow fibers recorded from the marked area in (**a**). (**d,e**) Fast fourier transformation (FFT) images of the marked areas of A and B in (**c**). The insets are the partial geometry models of anatase and rutile TiO_2, respectively. (**f,g**) The corresponding inverse fast fourier transformation (IFFT) images of (**d,e**), respectively. (**h,i**) The element mappings of Ti and O within a single nanofiber.

composed by Ti and O elements. The Cu and C signal should be from the TEM grid used to support the sample. The element mapping images of Ti (Fig. 3(h)) and O (Fig. 3(i)) exhibit a harmonious ravine distribution throughout the fiber body, verifying the hollow nature of the as-fabricated TiO_2 nanofibers.

Photocatalytic evolution of H_2 on the as-prepared products as well as P25 (the typical SEM image and EDX spectrum, see Figure S3, Supplementary Information) is carried out by using methanol as sacrificial agents and irradiation under a 300 W Xenon arc lamp. Figure 4(a) plots the typical H_2 evolution kinetic lines over these two photocatalysts. For the mesoporous TiO_2 hollow fibers, their photocatalytic reactions exhibit a stable H_2 release rate of ~499.1 μmol $g^{-1} \cdot h^{-1}$, which is much higher than that of P25 (*i.e.*, 197.8 μmol $g^{-1} \cdot h^{-1}$) and those reported for solid and porous TiO_2 nanofibers always lower than 400 μmol $g^{-1} \cdot h^{-1}$ (see Table 1). In order to investigate their reusability, these two photocatalysts are recovered and re-used for photocatalytic H_2 production under the identical experimental conditions. As shown in Fig. 4(b), the activity of the mesoporous TiO_2 hollow fibers is still maintained with no noticeable decrease observed after 3 cycles. However, the photocatalytic ability of P25 has evidently
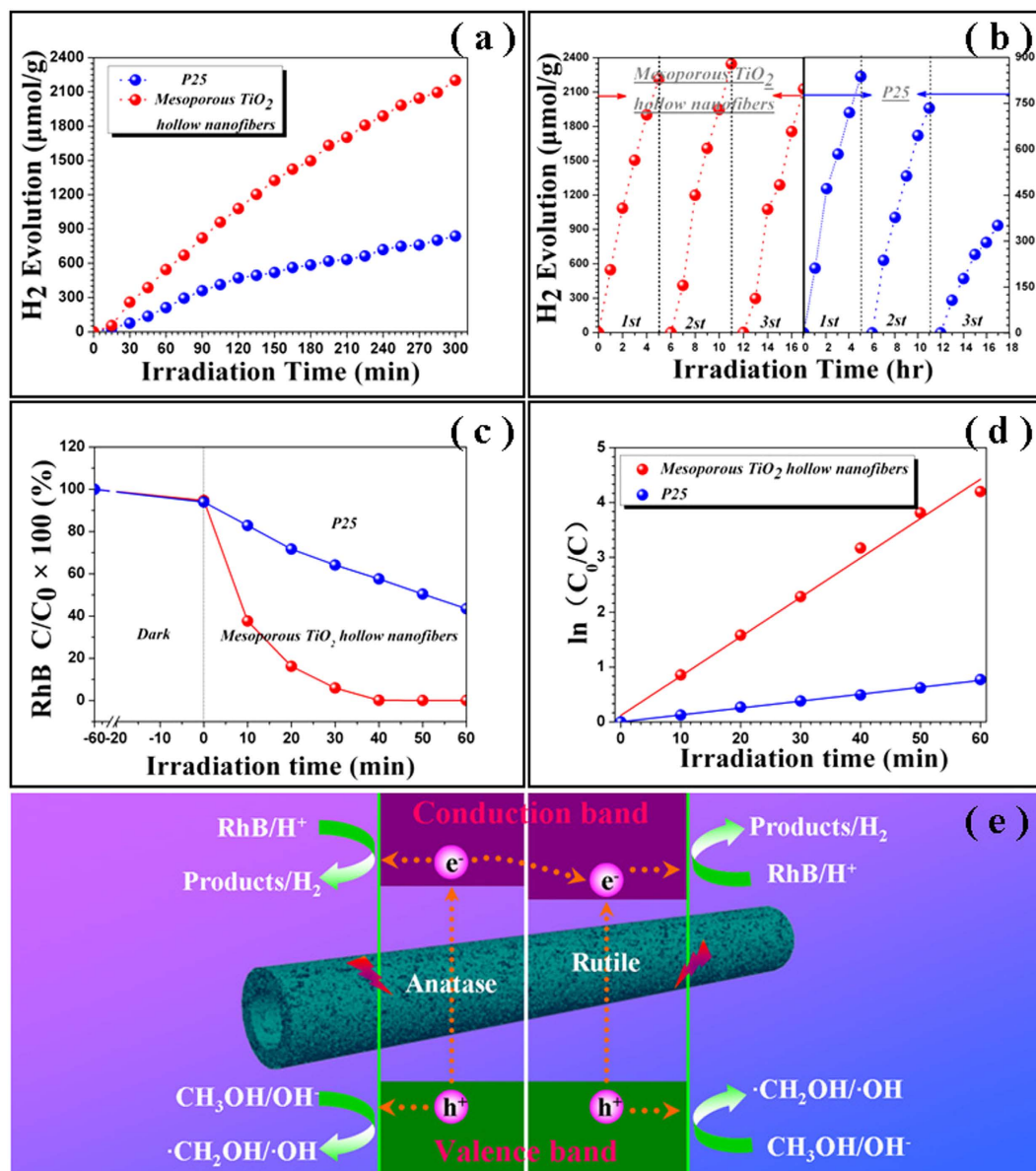
Figure 4. (**a**) The hydrogen production photocatalyzed by the as-fabricated mesoporous TiO$_2$ hollow nanofibers as well as p25 under different irradiation times. (**b**) Reusability experiment for photocatalytic H$_2$ generation of mesoporous TiO$_2$ hollow nanofibers and p25. (**c**) Photocatalytic degradation of RhB (C0 = 10 mg/L) of mesoporous TiO$_2$ hollow nanofibers and p25 under UV-visible light irradiation. (**d**) The plot of ln(C0/C) with irradiation time for mesoporous TiO$_2$ hollow nanofibers and p25. (**e**) The proposed mechanism for the enhanced photocatalytic activities of the mesoporous TiO$_2$ hollow fibers with mixed phases of anatase and rutile.

declined after 3 cycles. Obviously, the 1D mesoporous hollow structure exhibits a much better long-term photocatalytic stability than the commercial P25. Additionally, the photocatalytic properties of the as-prepared TiO$_2$ hollow nanofibers are evaluated by the decomposition of RhB dye. Figure 4(c) shows their time-dependent degradation of RhB, which are monitored by the maximum band absorbance (also see Figure S4, Supplementary Information), and corrected one by one based on the standard plots of the dye with various RhB concentrations (see Figure S5, Supplementary Information). It seems that, without the light irradiation, the concentration of RhB suspension over the mesoporous TiO$_2$ hollow fibers as well as P25 undergoes a tiny change during 60 min magnetic stirring for the sample preparation, suggesting that the dark physics adsorption have little influence on the dye concentration change. The colors of the suspensions catalyzed by the mesoporous TiO$_2$ hollow products (the inset in Figure S4(a), Supplementary Information) change gradually from pink to almost colorless, implying the nearly complete photodegradation of RhB. Nevertheless, the suspensions catalyzed by P25 (the inset of Figure S4(b), Supplementary Information) still maintain an obvious light pink color after 60 min illumination,

Material	Preparation	Morphology	Irradiation conditions	Reaction solution	Activity (μmol g^{-1}h^{-1})	Reference
TiO$_2$ (B)	hydrothermal	Nanofibers	15 W UV lamp	Neat ethanol	238	34
TiO$_2$	Electrospinning	Nanofibers	450 W Hg	Water+MeOH	54	20
TiO$_2$ (B)/Pt	hyndrothermal	Nanofibers	15 W UV lamp	Neat ethanol	257	35
TiO$_2$/Pt	Electrospinning	Nanofibers	300 W Xe	Water+MeOH	910	36
TiO$_2$/Pt	hydrothermal	Nanofibers	300 W Hg	Water+MeOH	310	37
TiO$_2$	hydrothermal	Nanofibers	6 UVB lamps	Water +ethanol	30	28
TiO$_2$	Electrospinning	Porous Nanofibers	400 W Hg	Water+MeOH	80	17
TiO$_2$	Electrospinning	Nanofibers	400 W Hg	Water+AO7	21	38
TiO$_2$	Electrospinning	Porous fibers	300 W Xe	Water+MeOH	198	27
TiO$_2$	foaming-assisted electrospinning	Mesoporous nanofibers	300 W Xe	Water+MeOH	399	29
TiO$_2$	foaming-assisted electrospinning	Mesoporous nanofibers	300 W Xe	Water+MeOH	499	Current work

Table 1. Comparison of the related typical works for H$_2$ production using TiO$_2$ nanofibers as the Photocatalyst.

declaring that the some part of the RhB still remained in the suspension without decomposition. The overall degradation efficiency is 99.5% for mesoporous TiO$_2$ hollow fibers, which is ~2.5 times to that of P25. To further study the photocatalytic reaction, the pseudo-first-order kinetic model is adopted according to the equation $ln(C_0/C) = k$, where C_0 is the adsorption equilibrium concentration of pollutant before irradiation, C is the instantaneous concentration, and k is the apparent rate constant with determined reaction time, respectively[5,26]. As shown in Fig. 4(d), the corresponding reaction rate constants (k) are calculated to be 0.071 and 0.010 min^{-1} for the mesoporous TiO$_2$ hollow fibers and P25, respectively. Notably, the present mesoporous hollow products own superior photodegradation efficiency to that of P25. These experimental results verify that, in comparison to the commercial products of P25, the present mesoporous TiO$_2$ hollow fibers could be a much higher efficient photocatalyst candidate for both photocatalytic evolution H$_2$ production and degradation of hazardous materials.

Discussion

The growth of mesoporous TiO$_2$ hollow fibers could be assigned to follow issues: i) The formation of the hollow interior. As stated in the experimental procedure, the used raw materials of PVP, TBOT, DIPA, absolute ethyl alcohol, CTAB and paraffin oil would cause the formation of microemulsions. As schematically illustrated in Fig. 1(a), the core-shell structure of the as-spun polymeric fibers would be then formed, due to the distinctively different phase interfaces between the mixtures dissolved in the solvent, which cause the formation of a core-shell jet driven by the electrical forces during electrospinning[27]. The core is mainly made up by the trapped paraffin oil, and the shell should be the remained materials of PVP/TBOT/CTAB/DIPA. Once subjected to be calcined at high temperature, the inside paraffin oil core would be completely decomposed into gas phases such as CO$_2$ and H$_2$O, leading to the formation of the hollow interior of the fiber. ii) The formation of the thoroughly mesoporous walls of the hollow fibers. It should be mainly ascribed to the thermal decomposition of foaming agents of DIPA assembled within the fibers, which would be converted into abundant vapor phases such as CO$_2$, NO$_2$ and H$_2$O[28], making the creation of mesoporous throughout the walls of the hollow fibers.

To account for the enhanced photocatalytic ability mesoporous TiO$_2$ hollow fibers, a tentative mechanism is proposed, as schematically illustrated in Fig. 4(e). It is well known that the crystallite phase and material architecture play a significant role on the photocatalytic performance of TiO$_2$ photocatalysts[2,3,29]. Thus, the excellent photocatalytic performance of mesoporous TiO$_2$ hollow fibers might be explained by the following points. i) The mixed phases of anatase and rutile TiO$_2$ within the fibers. The present products possess the similar functional mix-phase junction of P25, which leads to the improvement of interfacial charge transfer and effectively limits the charge recombination[20–22]. ii) The well-defined hollow mesoporous nanofibers. The presence of favorable hollow formation with big inner diameters could make the reactant more and easier to contact the photocatalysts, owing to the more active sites offered by the larger exposed surface areas[30,31]. iii) The 1D mesoporous architecture walls. This can not only remarkably inhibit the agglomeration of nanoparticles, but also improve the surface adsorption capacity of the reactants. Furthermore, the mesoporous channels existed throughout the fiber bodies also could facilitate the effective transportation of products[32,33]. In brief words, the as-fabricated mesoporous TiO$_2$ hollow fibers could be considered as the assembly of P25 nanoparticles with the mixed phases of anatase and rutile phases into hollow one-dimensional counterparts with thoroughly mesoporous walls, which offer the platform for synergetic combination of the mix-phase composition, hollow architecture and mesoporous walls to bring a significant enhancement on the photocatalytic activities.

Conclusions

In summary, we have demonstrated the investigation of mesoporous TiO_2 hollow nanofiber photocatalysts, which are fabricated via a facile single capillary electrospinning technique[39–41]. The obtained fibers are composed of anatase and rutile mixed phases with well-defined hollow bodies and thoroughly mesoporous walls. The as-fabricated mesoporous TiO_2 hollow fibers exhibit efficient photocatalytic activities and robust stabilities toward the hydrogen evolution and degradation of RhB, which are ~2.5 times to those of commercial P25, suggesting their promising applications as excellent photocatalysts. It is promising that the mesoporous TiO_2 hollow nanofibers could offer an ideal platform for synergetic combination of the mixed-phase composition, hollow architecture and mesoporous walls for the desired excellent photocatalytic efficiency and stability, which could provide a novel strategy for the exploration of novel TiO_2 photocatalysts with high performances.

References

1. Pang, C. L., Lindsay, R. & Thornton, G. Structure of clean and adsorbate-covered single-crystal rutile TiO_2 surfaces. *Chem. Rev.* **113,** 3887–3948 (2013).
2. Hisatomi, T., Kubota, J. & Domen, K. Recent advances in semiconductors for photocatalytic and photoelectrochemical water splitting. *Chem. Soc. Rev.* **43,** 7025–7035 (2014).
3. Linsebigler, A. L., Lu, G. & Yates, J. T., Jr. Photocatalysis on TiO_2 surfaces: principles, mechanisms, and selected results. *Chem. Rev.* **95,** 735–758 (1995).
4. Chen, H., Nanayakkara, C. E. & Grassian, V. H. Titanium dioxide photocatalysis in atmospheric chemistry. *Chem. Rev.* **112,** 5919–5948 (2012).
5. Zhang, L. *et al.* Heterojunctions in g-C_3N_4/TiO_2 (B) nanofibres with exposed (001) plane and enhanced visible-light photoactivity. *J. Mater. Chem. A* **2,** 2071–2078 (2014).
6. Hurum, D. C., Agrios, A. G., Gray, K. A., Rajh, T. & Thurnauer, M. C. Explaining the enhanced photocatalytic activity of Degussa P25 mixed-phase TiO_2 using EPR. *J. Phys. Chem. B* **107,** 4545–4549 (2003).
7. Yang, D. *et al.* An efficient photocatalyst structure: TiO_2 (B) nanofibers with a shell of anatase nanocrystals. *J. Am. Chem. Soc.* **131,** 17885–17893 (2009).
8. Yang, D. *et al.* Enhancing photoactivity of TiO_2 (B)/anatase core–shell nanofibers by selectively doping cerium ions into the TiO_2 (B) core. *Chem. Eur. J.* **19,** 5113–5119 (2013).
9. Zhang, L. *et al.* Heterojunctions in g-C_3N_4/TiO_2 (B) nanofibres with exposed (001) plane and enhanced visible-light photoactivity. *J. Mater. Chem. A* **2,** 2071–2078 (2014)
10. Zhang, S. *et al.* Enhanced photodynamic therapy of mixed phase TiO_2 (B)/anatase nanofibers for killing of HeLa cells. *Nano Res.* **7,** 1659–1669 (2014).
11. Wang, R., *et al.* Tuning and understanding the phase interface of TiO_2 nanoparticles for more efficient lithium ion storage. *Nanoscale,* doi: 10.1039/C5NR02582F (2015).
12. Hoyer, P. Semiconductor nanotube formation by a two-step template process. *Adv. Mater.* **8,** 857–859 (1996).
13. Kasuga, T., Hiramatsu, M., Hoson, A., Sekino, T. & Niihara, K. Titania nanotubes prepared by chemical processing. *Adv. Mater.* **11,** 1307–1311 (1999).
14. Rao, C., Govindaraj, A., Deepak, F. L., Gunari, N. & Nath, M. Surfactant-assisted synthesis of semiconductor nanotubes and nanowires. *Appl. Phys. Lett.* **78,** 1853–1855 (2001).
15. Goldberger, J. *et al.* Single-crystal gallium nitride nanotubes. *Nature* **422,** 599–602 (2003).
16. Martinson, A. B., Elam, J. W., Hupp, J. T. & Pellin, M. J. ZnO nanotube based dye-sensitized solar cells. *Nano Lett.* **7,** 2183–2187 (2007).
17. Lee, S. S., Bai, H., Liu, Z. & Sun, D. D. Electrospun TiO_2/SnO_2 nanofibers with innovative structure and chemical properties for highly efficient photocatalytic H_2 generation. *Int. J. Hydrogen Energy* **37,** 10575–10584 (2012).
18. Lin, H. P., Mou, C. Y. & Liu, S. B. Formation of mesoporous silica nanotubes. *Adv. Mater.* **12,** 103–106 (2000).
19. Yu, D. *et al.* Mesoporous nanotubes of iron phosphate: synthesis, characterization, and catalytic property. *Langmuir* **23,** 382–386 (2007).
20. Chuangchote, S., Jitputti, J., Sagawa, T. & Yoshikawa, S. Photocatalytic activity for hydrogen evolution of electrospun TiO_2 nanofibers. *ACS Appl. Mater. Inter.* **1,** 1140–1143 (2009).
21. Xiang, H. *et al.* A novel and facile method to prepare porous hollow CuO and Cu nanofibers based on electrospinning. *Cryst Eng Comm* **13,** 4856–4860 (2011).
22. Hua, G., Zhang, L., Fei, G. & Fang, M. Enhanced catalytic activity induced by defects in mesoporous ceria nanotubes. *J. Mater. Chem.* **22,** 6851–6855 (2012).
23. Ohno, T., Tokieda, K., Higashida, S. & Matsumura, M. Synergism between rutile and anatase TiO_2 particles in photocatalytic oxidation of naphthalene. *Appl. Catal., A* **244,** 383–391 (2003).
24. Li, G. *et al.* Synergistic effect between anatase and rutile TiO_2 nanoparticles in dye-sensitized solar cells. *Dalton Trans.* **45,** 10078–10085 (2009).
25. Kho, Y. K. *et al.* Photocatalytic H_2 evolution over TiO_2 nanoparticles. The synergistic effect of anatase and rutile. *J. Phys. Chem. C* **114,** 2821–2829 (2010).
26. Chen, W. *et al.* Enhanced visible-light activity of titania via confinement inside carbon nanotubes. *J. Am. Chem. Soc.* **133,** 14896–14899 (2011).
27. Hou, H. *et al.* Fabrication of porous titanium dioxide fibers and their photocatalytic activity for hydrogen evolution. *Int. J. Hydrogen Energy* **39,** 6837–6844 (2014).
28. Wu, M. C. *et al.* Enhanced photocatalytic activity of TiO_2 nanofibers and their flexible composite films: Decomposition of organic dyes and efficient H_2 generation from ethanol-water mixtures. *Nano Res.* **4,** 360–369 (2011).
29. Hou, H. *et al.* General strategy for fabricating thoroughly mesoporous nanofibers. *J. Am. Chem. Soc.* **136,** 16716–16719 (2014).
30. Zhan, S., Chen, D., Jiao, X. & Tao, C. Long TiO_2 hollow fibers with mesoporous walls: sol-gel combined electrospun fabrication and photocatalytic properties. *J. Phys. Chem. B* **110,** 11199–11204 (2006).
31. Zhang, X., Thavasi, V., Mhaisalkar, S. & Ramakrishna, S. Novel hollow mesoporous 1D TiO_2 nanofibers as photovoltaic and photocatalytic materials. *Nanoscale* **4,** 1707–1716 (2012).
32. Yu, J. C., Wang, X. & Fu, X. Pore-wall chemistry and photocatalytic activity of mesoporous titania molecular sieve films. *Chem. Mater.* **16,** 1523–1530 (2004).
33. Zhou, W. *et al.* Ordered mesoporous black TiO_2 as highly efficient hydrogen evolution photocatalyst. *J. Am. Chem. Soc.* **136,** 9280–9283 (2014).

34. Lin, C. H., Chao, J. H., Liu, C. H., Chang, J. C. & Wang, F. C. Effect of calcination temperature on the structure of a Pt/TiO$_2$ (B) nanofiber and its photocatalytic activity in generating H$_2$. *Langmuir* **24,** 9907–9915 (2008).
35. Wang, F. C., Liu, C. H., Liu, C. W., Chao, J. H. & Lin, C. H. Effect of Pt loading order on photocatalytic activity of Pt/TiO$_2$ nanofiber in generation of H$_2$ from neat ethanol. *J. Phys. Chem. C* **113,** 13832–13840 (2009).
36. Choi, S. K., Kim, S., Lim, S. K. & Park, H. Photocatalytic comparison of TiO$_2$ nanoparticles and electrospun TiO$_2$ nanofibers: effects of mesoporosity and interparticle charge transfer. *J. Phys. Chem. C* **114,** 16475–16480 (2010).
37. Li, W. *et al.* Single-crystalline and reactive facets exposed anatase TiO$_2$ nanofibers with enhanced photocatalytic properties. *J. Mater. Chem.* **21,** 6718–6724 (2011).
38. Lee, S. S., Bai, H., Liu, Z. & Sun, D. D. Novel-structured electrospun TiO$_2$/CuO composite nanofibers for high efficient photocatalytic cogeneration of clean water and energy from dye wastewater. *Water Res.* **47,** 4059–4073 (2013).
39. Seo, M., Kim, S. K., Han, J. H. & Hwang, C. S. Permittivity enhanced atomic layer deposited HfO$_2$ thin films manipulated by a rutile TiO$_2$ interlayer. *Chem. Mater.* **22,** 4419–4425 (2010).
40. Chen, H. *et al.* Fabrication of hierarchically porous inorganic nanofibers by a general microemulsion electrospinning approach. *Small* **7,** 1779–1783 (2011).
41. Chen, X. & Mao, S. S. Titanium dioxide nanomaterials: synthesis, properties, modifications, and applications. *Chem. Rev.* **107,** 2891–2959 (2007).

Acknowledgements

Author Contributions

W.L., B.T. and W.Y. conceived and directed the experiments. H.H., M.S. and L.W. performed the experiments. H.H., B.T. and W.Y. co-wrote the manuscript. All authors discussed the results and helped with the preparation of the final manuscript.

Additional Information

Supplementary information accompanies this paper at http://www.nature.com/srep

Competing financial interests: The authors declare no competing financial interests.

How to cite this article: Hou, H. *et al.* Efficient Photocatalytic Activities of TiO$_2$ Hollow Fibers with Mixed Phases and Mesoporous Walls. *Sci. Rep.* **5**, 15228; doi: 10.1038/srep15228 (2015).